CI&CEQ
Chemical Industry & Chemical Engineering Quarterly

Available online at
Association of the Chemical Engineers of Serbia AChE
www.ache.org.rs/CICEQ

Chem. Ind. Chem. Eng. Q. 29 (3) 209–224 (2023) CI&CEQ

LUCAS OLIVEIRA CARDOSO[1]
BRUNO SANTOS CONCEIÇÃO[1]
MÁRCIO LUIS LYRA PAREDES[2]
SILVANA MATTEDI[1]

[1]Chemical Engineering Graduate Program (UFBA/UNIFACS), Polytechnic School, Federal University of Bahia, Salvador, BA, Brazil

[2]Chemical Engineering Graduate Program, Rio de Janeiro State University, Rio de Janeiro, RJ, Brazil

SCIENTIFIC PAPER

UDC 544.6:66:004

THERMODYNAMIC MODELING OF GAS SOLUBILITY IN IONIC LIQUIDS USING EQUATIONS OF STATE

Article Highlights

- The SRK expressed the same behavior as the CPA EoS for the properties of pure ionic liquids
- The change of the associative schemes did not present differences for pure ILs for CPA EoS
- PC-SAFT with the 4C associative scheme presented the best fit for both pure ionic liquids
- [OMIM][NTf_2] with CO_2 and H_2S had as best models PC-SAFT (4C) and CPA (2B), respectively
- For [EMIM][TfO] with CH_4, CO_2 and H_2S were CPA (NA), PC-SAFT (4C), and SRK, respectively

Abstract

This work aimed at the thermodynamic modeling of gas solubility in ionic liquids (ILs) using the Soave-Redlich-Kwong (SRK), cubic-plus-association (CPA), and perturbed-chain statistical associating fluid theory (PC-SAFT) equations of state. Wherefore, the routines were developed for the parameterization of ILs. Then, the ILs were implemented in the Aspen plus simulator to evaluate the equations of state and explore the phase equilibrium data with the predictive equations and the correlation of the binary interaction parameter. Hence, it was verified the correlation of the density and speed of sound curves presented limitations to correcting the slope of the curves of pure ILs. Nonetheless, the PC-SAFT with the 4C associative scheme demonstrated a better fit for the thermophysical properties. As for the prediction of phase equilibrium for the [EMIM][TfO], the PC-SAFT with the 2B scheme showed a better fit with CO_2, while the CPA with the 2B scheme presented the best result for H_2S. For [OMIM][NTf_2], the PC-SAFT with the 1A scheme showed better results with CO_2, and the CPA with the 2B scheme showed the lowest deviation with H_2S.

Keywords: thermodynamic modeling, ionic liquids, equations of state, associating, Aspen plus.

Natural gas is a fossil fuel formed by a multicomponent mixture, in which it contains methane and other higher alkanes in lesser amounts, as well as acid gases such as carbon dioxide (CO_2) and hydrogen sulfide (H_2S), nitrogen (N_2), mercaptans, carbonyl sulfide, organic sulfides, and water (H_2O) [1,2].

Moreover, natural gas is a valuable energy source, which can be highlighted as a source of energy for industries and domestic applications due to its abundance and low cost [3], as it is also considered a non-polluting energy source, being in opposition to other fuels [4,5]. Thus, using natural gas in contrast to coal and oil emerges as a less polluting and significant alternative for energy security.

The extracted raw gas is often saturated by a steam of water [6]. Hence, to prevent the formation of

Correspondence: S. Mattedi, Chemical Engineering Graduate Program (UFBA/UNIFACS), Polytechnic School, Federal University of Bahia, Salvador, BA, Brazil.
E-mail: silvana@ufba.br
Paper received: 17 April, 2022
Paper revised: 6 September, 2022
Paper accepted: 29 October, 2022

https://doi.org/10.2298/CICEQ220417028C

hydrates and acids due to the presence of carbon dioxide (CO_2) and hydrogen sulfide (H_2S), the water (H_2O) and these gases present in natural gas must be removed, being that these components are alarming due to their negative consequences for humans, equipment, and the environment [5,7]. Among acid gases, H_2S is a very toxic and corrosive contaminant, which can cause various diseases and even death in specific concentrations. Besides, it is noteworthy that the presence of CO_2 contributes to the decrease in the heat capacity of natural gas and the performance of liquefaction processes [5,8,9].

In recent decades, the development of sustainable alternative technologies through green chemistry practices led to the design of solvents with lower environmental impact, such as ionic liquids (ILs). The ILs are salts of organic cations and inorganic or organic anions. The presence of bulky and asymmetric ions concerning single ions of inorganic salts results in a melting point below 100 °C [10]. They have excellent physical, biological, and chemical properties due to their good thermal capacity and low volatility. Hence, they are also safe to manage compared to mineral acids, have high thermal stability compared to commonly used organic solvents, and have a wide adjustable range of acidity, basicity, and solubility in the organic and aqueous solvents [11]. In this way, ILs can offer unique selectivity and replace conventional solvents [12].

In this sense, separation processes aim to obtain a product with greater added value and less environmental impact. In recent years, ILs began to be investigated for the removal of acid gas present in natural gas [4]. For example, Jalili *et al.* [13] observed the solubility of CO_2 is higher in ILs with -CF3 and [NTf_2]- groups. Meanwhile, Nematpour *et al.* [14] analyzed fluorinated-based ILs and found that [EMIM][TfO] had the potential to be used to separate CO_2 and H_2S from each other. Also, Haider *et al.* [4] showed in their review the effectiveness of CO_2 and H_2S separation following the trend of [EMIM][FAP] > [BMIM][PF_6] > [OMIM][NTf_2]. So, the description of the phase equilibria is of great interest for the design, simulation, and optimization of these processes. Consequently, a good selection and parameterization of the thermodynamic model become essential steps for the reliable representation of the process.

The simulation of the process allows a better understanding of the environment under analysis, identifying problems, formulating strategies, and identifying opportunities for system improvements. Hence, one of the most used commercial process simulators in the chemical and petroleum industry is ASPEN (Advanced System for Process Engineering), which has a wide library of properties, many thermodynamic models, and tools for the design, simulation, and analysis of components, and equipment [15,16]. On this wise, with the support of the Aspen Plus® process simulator, it was possible to study the properties modeling of associative systems due to its robustness for solving the equations of state present in the simulator.

The goal of this work was to develop thermodynamic modeling using ILs as a solvent to remove acid gases present in natural gas and its application in the Aspen Plus simulator in the analysis of the solubility of ILs, methane, and acid gases. Thus, this work consisted of the thermodynamic modeling of the pure and binary components through the thermodynamic models SRK, CPA, and PC-SAFT based on experimental data from the literature. Furthermore, ILs were parameterized and added to Aspen Plus by Aspen Technology®, as they are not present in the database.

Equations of state

Equations of State (EoS) are used for calculations of thermodynamic properties of pure substances and mixtures in industry and academia, especially for systems at high pressure. The term "high pressure" refers to pressures high enough to significantly change the thermodynamics of the system [17]. The traditional way to extend the application of the EoS to mixtures is using mixing rules, i.e., mathematical expressions that propose the dependence of the EoS on the concentration of species [18].

In this present work, the Soave-Redlich-Kwong (SRK), cubic-plus-association (CPA), and perturbed-chain statistical associating fluid theory (PC-SAFT) EoS were studied to evaluate the representations of the vapor-liquid equilibrium involving acid gases and ILs.

SRK EoS

The SRK EoS appeared in 1972 when Giorgio Soave realized that although the Redlich-Kwong equation (1949) could be applied to calculate with a good degree of accuracy, the volumetric and thermal properties of pure compounds and mixtures often presented poor results for calculations of gas-liquid equilibrium (GLE) of multicomponent mixtures [19]. Nevertheless, it is widely applied in the oil and gas industry, in addition to being widely applied for nonpolar mixtures, for example, hydrocarbons. So, for further details concerning the description of terms and their application related to the SRK, it is recommended to consult the basic works [19–21].

CPA EoS

The CPA was developed by Kontogeorgis *et al.*

[22] to give an EoS suitable for associative fluids and their mixtures based on perturbation theory, which could extend to compounds with hydrogen bonding (polar), thus attending a variety of systems of interest to the oil and gas industry (hydrocarbons, gases, water, alcohols, and glycols). Furthermore, it would be possible to evaluate the performance correlating the vapor pressures of pure compounds and densities in the liquid phase [23].

The CPA EoS can be expressed in terms of pressure as a sum of the SRK cubic equation and the contribution of the association term in the form provided by Michelsen and Hendriks [23].

$$P = \frac{R\,T}{V_m - b} - \frac{a(T)}{V_m\,(V_m + b)} - \frac{1}{2}\left(\frac{R\,T}{V_m}\right)\left(1 + \frac{1}{V_m}\frac{\partial \ln g}{\partial\left(\frac{1}{V_m}\right)}\right) \sum_i x_i \sum_{A_i}(1 - X_{Ai}) \quad (1)$$

Hence, for further details concerning the description of terms and their application related to the CPA EoS, it is recommended to consult the basic works [22–24].

PC-SAFT EoS

The PC-SAFT EoS, one of the most prevalent versions of the Statistical Associating Fluid Theory (SAFT) EoS, was pioneered by Gross and Sadowski [25], providing reliable and applicable thermodynamics to model thermodynamic properties of many systems, especially systems that are asymmetric in size [26]. Additionally, the PC-SAFT model proved suitable for pure components and mixtures involving solvents and gases, covering liquid-liquid equilibrium (LLE) and GLE of polymeric systems [27].

The main idea of the perturbation theory is to divide molecular interactions into main and additional contributions, such as attraction and repulsion. The attractive part is divided into dispersive and associative interactions. Meanwhile, the repulsive part is described by the hard-chain term derived from Chapman *et al.* [28], which contains the terms hard-sphere and chain [27], which uses another perturbation theory to include softness in this reference potential.

$$\tilde{a}^{res} = \tilde{a}^{hs} + \tilde{a}^{chain} + \tilde{a}^{disp} + \tilde{a}^{assoc} \quad (2)$$

The $\tilde{a}^{res}$ represents the residual Helmholtz energy, the $\tilde{a}^{hs}$ represent the contribution of the hard-sphere Helmholtz energy term, the $\tilde{a}^{chain}$ represents the chain Helmholtz energy, the $\tilde{a}^{disp}$ represents the energy of dispersive Helmholtz and, finally, the $\tilde{a}^{assoc}$ represents the associative Helmholtz energy. For further details concerning the description of terms and their application related to the PC-SAFT EoS, it is recommended to consult the basic works [24,25,27–29].

For the thermodynamic modeling of ILs and acid gases, the SRK, CPA, and PC-SAFT equations of state were used to verify the improvements in calculating the properties of pure components and binaries mixtures. Furthermore, knowing that the SRK can be interpreted as a model for attractive spheres based on the repulsive potential of hard spheres plus dispersive forces, the CPA includes the contribution of SRK plus an association term and, finally, the PC-SAFT, which attractive part also contains an associative term, and terms for chains of segment interacting but a softened repulsive term plus a better-defined attractive dispersion term [25].

Nevertheless, as the vapor pressure of ILs is low and there are usually few available data, this property is difficult to apply to the parametrization of ILs. In this way, Loreno *et al.* [30] developed a methodology using density and speed of sound in the adjustment of the parameters of the pure components with the GC-s-PC-SAFT (Group Contribution Simplified Perturbed Chain Statistical Associating Fluid Theory). However, their work was restricted to assessing the equilibrium of ionic liquid + carbon dioxide and ionic liquid + methane. For this reason, it justifies the emergence of interest in evaluating other thermodynamic models with different associative types for the evaluation of acid gases and, thus, be applied to the calculation of the solubility of ILs and acid gases present in natural gas. Also, those authors did not employ a commercial simulator in their calculations, which is an objective of this work.

METHODOLOGY

ILs

In this work, two fluorinated ILs that dissolve acid gases were selected: 1-ethyl-3-methylimidazolium trifluoromethanesulfonate [EMIM][TfO] (CAS: 145022-44- 2) and 1- octyl- 3- methylimidazolium bis(trifluorom ethyl)sulfonylimide [OMIM][NTf_2] (CAS: 178631-04-4). Therefore, it was necessary to obtain experimental data, such as density (ρ), speed of sound (u), liquid heat capacity at constant pressure (C_p^{liq}), for pure ILs and the GLE with acid gases and methane for evaluation. For the first IL, the experimental data were taken from Vercher *et al.* [31], while the GLE data were obtained from Nematpour *et al.* [14] for [EMIM][TfO]/CO_2 and [EMIM][TfO]/H_2S and from Lee [32] for [EMIM][TfO]/CH_4. For the second IL, the experimental data and the GLE data for [OMIM][NTf_2]/CO_2 and [OMIM][NTf_2]/H_2S were taken

from Zorębski *et al.* [33] and Jalili *et al.* [13], respectively.

Thermodynamic modeling

The comparison between the experimental data and those calculated by the EoS was performed by calculating the absolute average relative deviation (AARD), which is provided as a percentage from Eq. (3):

$$AARD(\%) = \frac{1}{n}\sum_{i=1}^{n}\left|\frac{v_i^{\exp} - v_i^{cal}}{v_i^{\exp}}\right| 100 \quad (3)$$

Therefore, the estimation of the parameters took place through the minimization of the objective function (F_{obj}), defined as the weighted sum of squares by the experimental uncertainties in density and speed of sound, according to Eq. (4):

$$F_{obj} = \sum_{i=1}^{n}\left(\frac{\rho_i^{cal} - \rho_i^{\exp}}{\delta\rho^{\exp}}\right)^2 + \left(\frac{u_i^{cal} - u_i^{\exp}}{\delta u^{\exp}}\right)^2 \quad (4)$$

The Swarm method proposed by Kennedy and Eberhart [34] was used to estimate the parameters of the EoS, which iteratively optimizes a problem to improve the candidate solution and then applies lower and upper bounds to obtain better estimates of the parameters. In line with this, the Simplex method described by Nelder and Mead [35] was used to minimize the objective function using the best candidate obtained with the Swarm method since performing this procedure improves the adjustment of the estimated parameters. Finally, the methodology proposed by Topliss *et al.* [36] was used to solve the problem of finding roots of a non-cubic EoS, which reliably converges.

In this way, the program developed outside the Aspen plus simulator for estimating parameters from the density and speed of sound data has protections to guarantee the reliable resolution of the proposed problem.

SRK equation

The SRK EoS is calculated from P_c, T_c, and ω data [19], but for ILs, these experimental properties are difficult to obtain, as the degradation of the IL occurs before reaching the critical point. In this way, these parameters were obtained from the data a_0, b_{CPA}, and c_1 of the CPA EoS using density and speed of sound data. The model selected in the Aspen plus was the RK-Aspen (SRK), given that the physical part of the CPA EoS uses the c_1 function proposed by Graboski and Daubert [20].

In this wise, the calculation of T_{cm} was performed using the parameters a_0, b_{CPA} and c_1, which can be observed in Equation (5).

$$T_{cm} = \frac{\left(\frac{1+c_1}{c_1}\right)^2}{\left(\frac{1+m_m}{m_m}\right)^2}\ \frac{\Omega_B\ a_0}{\Omega_A\ R\ b_{CPA}} \quad (5)$$

Moreover, the terms m_m and P_{cm} were obtained according to Equations (6) and (7), respectively.

$$m_m = c_1\sqrt{\frac{a_0\ \Omega_B}{\Omega_A\ b_{CPA}\ R\ T_{cm}}} \quad (6)$$

$$P_{cm} = \Omega_B\ \frac{R\ T_{cm}}{b_{CPA}} \quad (7)$$

The parameters of the SRK equation were established considering $T_c^* = T_{cm}$,, $P_c^* = P_{cm}$ and the ω was obtained from the consideration of $m_m = c_1$, and, in this way, analytically solved the equation proposed by Graboski and Daubert [20] for obtaining the acentric factor. These results can be found in the Supplementary Material of this work.

CPA equation

The CPA EoS has five pure parameters for each component, in addition to the choice of associative type. In this sense, three parameters refer to the physical part (a_0, b_{CPA}, and c_1) and two parameters refer to the association (ϵ^{AB} and β^{AB}) [23]. The methodology is like the one applied to the SRK model of this present work, apart from the addition of associative parameters and the choice of associative type, in which parameterizations were conducted in this study using associative schemes 1A, 2B, 3B, and 4C. This work represents an engineering model using association to represent interactions in complex systems involving ILs, which are treated as neutral molecules. Thus, the schemes analyzed in this work correspond to the schemes present in the Aspen plus simulator, and the main discussions of the associative types can be seen elsewhere [24].

The parameters T_{cm}, m_m, and P_{cm} were calculated as shown in Eqs. (5) and (7), and the associative parameters ϵ^{AB} and β^{AB} were determined along with a_0, b_{CPA}, and c_1 according to the proposed methodology using density and spend of sound, the calculation memory can be found in the Supplementary Material of this work.

PC-SAFT

The PC-SAFT EoS for a non-associative substance necessarily requires three parameters (m_i,

σ_i, and ε_i) [25], while for the associative components, there are two additional parameters (ϵ^{AB} and K^{AB}), besides the choice of associative type [27]. According to the scenario presented for ILs concerning vapor pressure, the parameterization proposed for the PC-SAFT model follows similarly to the proposal for the CPA, based on the density and speed of sound data. Furthermore, the calculation memory can be found in the Supplementary Material of this work.

The associative term in the CPA and PC-SAFT demand two parameters, the associative energy and the associative volume. Moreover, these parameters may be highly correlated. Hence, in this study, some orders of magnitude for the associative volume were tested better to understand the effect of this parameter in the modeling.

Aspen plus simulator

ILs are compounds not presented in the Aspen plus database; therefore, for the simulation and analysis of pure and binary data, creating a component informing the structure and its properties in the software became necessary. In addition to informing the parameters of the components in the equations of state, it is necessary to add two properties that are ideal gas heat capacity (C_p^{gi}) and Antoine vapor pressure (P_{Ant}^{v}). Therefore, in this part, the PML equation (Modified API) was selected to adjust the C_p^{gi} of ILs, according to Equation (8).

$$C_P^{gi} = C_{1i} + C_{2i}T + C_{3i}T^2 - \frac{C_{4i}}{T^2} + \frac{C_{5i}}{T} \tag{8}$$

Another important property is the vapor pressure, which is required by the simulator, even if it is not applied in the tests. Thus, a very low value was fixed for the vapor pressure, and the Antoine equation was informed as $\ln(P_{Ant}^{v})$ = -10 with Antoine pressure in bars.

Another important part is the regression of parameters, which can be performed for pure components or mixtures. So, the regressed binary interaction parameters were obtained from phase equilibrium data, which equations are presented below for the SRK, CPA, and PC-SAFT, respectively.

The SRK model, when dealing with mixtures, uses the mixing rules suggested by Mathias [21]. Thus, the regressed parameters were k_{aij}^{0}, k_{aij}^{1}, k_{bij}^{0}, and k_{bij}^{1} as presented in Equations (9) and (10).

$$a = \sum_i \sum_j x_i\, x_j\, \sqrt{a_i\, a_j}\left(1 - k_{aij}^{0} - k_{aij}^{1}\, \frac{T}{1000}\right) \tag{9}$$

For CPA, the equation has two parameters for the k_{ij}, as shown in Equation (11).

$$k_{ij} = k_{ij}^{0} + k_{ij}^{1}\, \frac{T}{T_{ref=298.15\ \mathrm{K}}} \tag{11}$$

For PC-SAFT, the equation has five parameters for the k_{ij}, but the regression was performed only for two parameters, as shown in Equations (12).

$$k_{ij} = k_{ij}^{0} + k_{ij}^{1}\, \frac{T_{ref=298.15\ \mathrm{K}}}{T} \tag{12}$$

RESULTS AND DISCUSSION

Thermodynamic modeling of pure components

Parameters of gases for the EoS

The parameters of gases for the EoS were obtained from the literature [25,37–40]. The parameters of gases allowed the validation of the algorithm developed for estimating ILs parameters, which could calculate thermophysical properties and show excellent results. Vapor pressure data also are important for pure components. The thermodynamic models were compared with experimental data for CH_4, CO_2, and H_2S [41], as shown in the Supplementary Material.

Parameters of ILs for the EoS

For pure ILs, the parameters estimated from the liquid density and speed of sound data are presented for the SRK (RK-Aspen model in the Aspen plus simulator), CPA, and PC-SAFT equations of state in Tables 1, 2, and 3, respectively.

Thus, an aspect being observed is the estimation time of the ILs parameters that vary with the models and the amount of experimental data. For example, the [EMIM][TfO] presented seven experimental points for density, while the [OMIM][NTf_2] presented seventeen experimental points. Regarding the liquid heat capacity at constant pressure and speed of sound, the [EMIM][TfO] presented seven experimental points, and the [OMIM][NTf_2] presented twenty-two points. Estimation time and the used computer machine were reported in Supplementary Material.

For the non-associative CPA, three parameters were estimated, while in the associative CPA, five parameters were varied by fixing the values of β^{AB} and obtaining the other four parameters. Hence, when providing Aspen plus with the associative obtained outside the simulator, a limitation was discovered concerning the $\epsilon^{AB/R}$ parameter, in which values above $1.2{\cdot}10^4$ K led to errors in calculating pure components properties. In this way, it was verified that the gradual decrease of the parameter $\epsilon^{AB/R}$ did not affect the

Table 1. Estimated parameters of ILs for the SRK model.

Components	MM [g/mol]	T_c^* [K]	P_c^* [bar]	ω [-]
[EMIM][TfO]	260.23	1217.53	49.742	0.01164
[OMIM][NTf_2]	475.47	581.50	12.287	2.44405

Table 2. Estimated parameters of ILs for the CPA EoS.

		CPA					
Components	MM [g/mol]	m_m [-]	T_{cm} [K]	P_{cm} [bar]	ϵ^{AB}/Rb[K]	β^{AB} [-]	Associative types
[EMIM][TfO]	260.23	0.50313	1217.53	49.742			NA*
		0.66353	1050.84	42.929	9000.0	1	1A
		0.83466	916.68	37.446	9000.0	1	2B
		0.83466	916.68	37.446	9000.0	0.1	2B
		0.83466	916.68	37.446	9000.0	0.001	2B
		0.83466	916.68	37.446	9000.0	0.00001	2B
		0.83466	916.68	37.446	9000.0	1	3B
		1.21621	716.66	29.272	9000.0	1	4C
[OMIM][NTf_2]	475.47	3.34491	581.50	12.287			NA*
		3.59020	551.59	11.654	9000.0	1	1A
		3.85350	524.11	11.073	9000.0	1	2B
		3.85350	524.11	11.073	9000.0	0.1	2B
		3.85350	524.25	11.076	9000.0	0.001	2B
		3.85350	524.11	11.073	9000.0	0.00001	2B
		3.85386	524.09	11.072	9000.0	1	3B
		4.44497	475.55	10.045	9000.0	1	4C

*NA: Non-associative.

Table 3. Estimated parameters of ILs for the PC-SAFT EoS.

Components	MM [g/mol]	m [-]	σ [A]	$\frac{\varepsilon_{ij}}{k_b}$[K]	$\frac{\epsilon^{AB}}{k_b}$[K]	K^{AB} [-]	Associative types
[EMIM][TfO]	260.23	6.4888	3.5351	373.28			NA*
		6.9693	3.4466	345.90	9000.0	1	1A
		7.4774	3.3617	321.82	12122.6	1	2B
		7.4782	3.3615	321.80	12562.3	0.1	2B
		7.4777	3.3616	321.81	15055.6	0.001	2B
		7.4779	3.3616	321.81	17213.4	0.00001	2B
		7.4775	3.3617	321.82	7424.5	1	3B
		8.6163	3.1968	280.47	9000.0	1	4C
[OMIM][NTf_2]	475.47	9.6006	3.8578	355.48			NA*
		10.1783	3.7766	334.53	9000.0	1	1A
		10.8035	3.6957	315.22	9000.0	1	2B
		10.8035	3.6957	315.22	9000.0	0.1	2B
		10.8035	3.6957	315.22	9000.0	0.001	2B
		10.8035	3.6957	315.22	9000.0	0.00001	2B
		10.8035	3.6957	315.22	9000.0	1	3B
		12.5487	3.4980	275.55	9000.0	1	4C

*NA: Non-associative.

calculated pure component or mixture properties. Therefore, it was used a default value of $\epsilon^{AB/R}$ = 9000.0 K as the Aspen plus software performed the intended procedure correctly and reliably.

Like what was presented in the CPA EoS, the mentioned limitation with the parameter $\epsilon^{AB/kb}$ was also found when dealing with the PC-SAFT EoS. On the other hand, differently from what was presented for CPA, the PC-SAFT complications were found around $2{\cdot}10^4$ K. Therefore, the estimated values that were above the established limit were also empirically set to the value of $\epsilon^{AB/kb}$= 9000.0 K. The $\epsilon^{AB/kb}$ values that were below this limit were kept in estimated values. In this regard, another valuable piece of information to be

highlighted is that there is a relationship between the optimal values of $\epsilon^{AB/R}$ and β^{AB} for CPA and $\epsilon^{AB/kb}$ and K^{AB} for PC-SAFT, which values present inversely proportional relationships, thus, generating compensation in associative terms. This fact happens when the $\Delta^{Ai\,Bj}$ assumes sufficiently high values, and the results of interest in this paper are not sensitive to the associative parameters.

Another vital piece of information to be added to the Aspen plus is the C_p^{gi}, which was calculated from experimental data from C_p^{liq}, while C_p^{res} was calculated using the adjusted parameters. Thus, the parameters for the C_p^{gi} function of the mentioned software was obtained. The parameters applied can be found in the Supplementary Material of this present work for the respective thermodynamic models.

Properties calculations of pure ILs

It was analyzed that the non-association, the choice of the scheme, and the variation of the associative parameter did not influence the fit of the pure [EMIM][TfO] data using the SRK and CPA models, thus proving freedom for the model selection. Furthermore, it investigated the contribution of the term, and the selection of the associative scheme for the CPA EoS showed no differences in the density adjustment, leading to an AARD of 0.54%, as shown in Table 4.

Table 4. Absolute Average Relative Deviation (AARD) in percentage for thermophysical properties for SRK, CPA, and PC-SAFT models for [EMIM][TfO] and [OMIM][NTf$_2$].

	[EMIM][TfO]											
AARD (%)	Density						Speed of sound					
	SRK	NA*	1A	2B	3B	4C	SRK	NA*	1A	2B	3B	4C
SRK	0.54						1.95					
CPA		0.54	0.54	0.54	0.54	0.54		1.95	1.95	1.95	1.95	1.93
PC-SAFT		0.32	0.29	0.25	0.25	0.16		0.84	0.70	0.61	0.60	0.53
	[OMIM][NTf$_2$]											
AARD (%)	Density						Speed of sound					
	SRK	NA*	1A	2B	3B	4C	SRK	NA*	1A	2B	3B	4C
SRK	0.24						4.02					
CPA		0.24	0.24	0.24	0.24	0.25		4.05	4.09	4.09	4.09	4.16
PC-SAFT		0.20	0.17	0.13	0.13	0.07		1.00	0.93	0.87	0.87	0.75

In addition, analogously, the variation of the associative term demonstrates no difference in the adjustment of the density and speed of sound data as a function of temperature for the [EMIM][TfO] using the SRK, non-associative and associative CPA with 2B scheme, which presented AARD of 0.54% and 1.95% for density and speed of sound, respectively.

In agreement with the CPA EoS, the PC-SAFT did not show divergence in the selection of the associative parameter, thus allowing a wide choice of the associative parameter. Nonetheless, in the PC-SAFT EoS, the choice of the associative scheme influenced the adjustment of the pure component, in which there was a decrease in the AARD of the associative PC-SAFT compared to the non-associative one, in which the AARDs for density were 0.32 % for non-associative, 0.29% for 1A scheme, 0.25% 2B and 3B schemes, and 0.16% for 4C scheme, while for the speed of sound, the AARD was 0.84% for the non-associative PC-SAFT, 0.70% for 1A scheme, 0.61% 2B scheme, 0.60% for 3B scheme and 0.53% for the 4C scheme. Therefore, for the PC-SAFT EoS, the 4C scheme was the one that presented the best fit for the thermophysical properties of density and speed of sound due to the AARDs that were 0.16% and 0.53%, respectively.

Table 4 also presents the deviation for the density and speed of sound of the ionic liquid [OMIM][NTf$_2$] using SRK, CPA, and PC-SAFT models. Thus, from Table 4, it was found that for the density curve, there was no difference between SRK and non-associative and associative CPA EoS, which presented an AARD of 0.24%. However, regarding the speed of sound, the SRK model presented the lowest AARD, concluding that the contribution of the associative term did not improve the fit of the mentioned curve; thus, the lowest AARD was 4.02% for the SRK model.

On the other hand, PC-SAFT showed significant improvements in the adjustment of density curves. The non-associative PC-SAFT obtained a reduction of 0.04% compared to SRK and CPA. Moreover, PC-SAFT, with the 4C scheme in the associative term, led to the lowest AARD.

Finally, as shown for the other ionic liquid, the C_p^{liq} was adjusted from the calculation of the C_p^{res} of the respective equations of state to inform the C_p^{ig} in the Aspen plus, causing it to be adjusted the C_p^{liq}. Further details and information on the properties and parameters, and associative schemes are present in the Supplementary Material.

GLE results

Methane + [EMIM][TfO] equilibria results

The solubility calculation was carried out to

evaluate the thermodynamic models in predicting the solubility curves of methane, the main component of natural gas, in ILs so that it was possible to select the best thermodynamic model for this application.

At first, the solubility curves will be presented with the SRK and CPA (β^{AB}=1 for the associative ones) models in a predictive way, i.e., the binary interaction parameter equals zero (k_{ij}=0). In this way, Figure 1(a) shows far the predictive results were in comparison with the experimental data. Additionally, another model to be analyzed was PC-SAFT (K^{AB}=1 for associations), but initially, tests were performed with k_{ij}=-0.1, as shown in Figure 1(b). It is because it was not possible to converge the vapor-liquid equilibrium in the simulator with k_{ij}=0. In this way, an empirical adjustment was made for the binary interaction parameter.

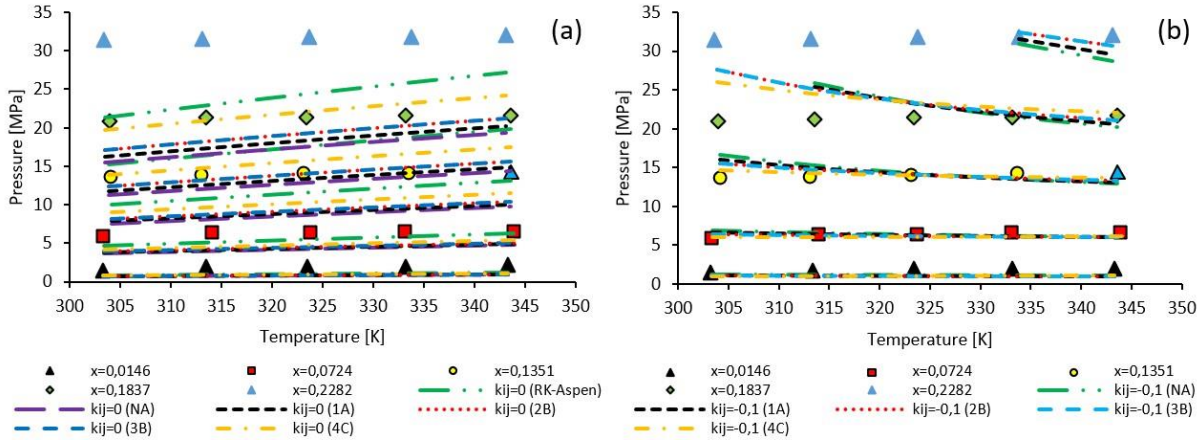

Figure 1. P-T results for CH_4 and [EMIM][TfO]: (a) Results with k_{ij}=0 for SRK and CPA for different associative schemes; (b) Results with k_{ij}=-0,1 for non-associative PC-SAFT and PC-SAFT for different associative schemes; Experimental data from Lee [32].

The AARD for SRK, CPA, and PC-SAFT models are included in the supplementary material. Thus, when analyzing, with k_{ij}=0, the SRK model showed the lowest AARD, 23.02%, which showed that the association for the IL did not enhance the prediction of the solubility of methane.

The equilibrium calculation outside the Aspen plus software allowed the convergence of equilibrium in conditions where there was no convergence in the simulator to the PC-SAFT EoS. The pressure values found were way higher than the experimental values. It is important to study other systems for which equilibrium data with other hydrocarbons are available, so a more comprehensive analysis can be conducted.

A regression of the binary interaction parameters was performed using two parameters (2p). Nevertheless, it is worth noting that concerning the SRK model, two binary interaction parameters were adjusted, one for the attractive parameter and another for the covolume parameter simultaneously, so for the SRK model, 2p represents the adjusted parameters k_{aij}^0 and k_{bij}^0, while 4p represents the adjusted parameters k_{aij}^0, k_{aij}^1, k_{bij}^0, and k_{bij}^1. In this way, the results were shown to improve significantly.

The models with two parameters showed AARD of 11.50% for SRK, 8.99% for CPA (NA), 9.12% for CPA (1A), 11.40% for PC-SAFT (NA), and 12.13% for PC-SAFT (1A), concluding that the CPA (NA) model presented the best fit with two parameters. Nevertheless, when considering the SRK model with four parameters, i.e., the parameter of binary interaction as a function of temperature for the attractive and covolume parameters, the latter presented the lowest AARD of 8.54%. More details of the AARD are in the Supplementary Material.

Carbon dioxide + ILs equilibria results

The solubility curves for CO_2 and [EMIM][TfO] are shown using the SRK model, presenting predictive results and the fit of the binary interaction parameters for the attractive and covolume parameters. As explained for methane, the adjustments 2p and 4p were performed for the parameter k_{ij}. Thus, Figure 2 shows a decrease in AARD by adding binary interaction parameters as a function of temperature, i.e., with four parameters.

The solubility curves for CO_2 and [EMIM][TfO] are shown using the CPA and PC-SAFT EoS to demonstrate that the variation of the associative parameter did not cause changes in the CPA and PC-SAFT curves, which can be verified in Figure 3(a) and Figure 3(b), respectively.

To improve the fits of the solubility curves and, thus, represent the experimental data more accurately, the binary interaction parameters of the CPA and PC-SAFT EoS were adjusted based on the equilibrium data of CO_2 and [EMIM][TfO]. Thus, the curves with 2 regressed parameters are shown in Figure 3(c) and

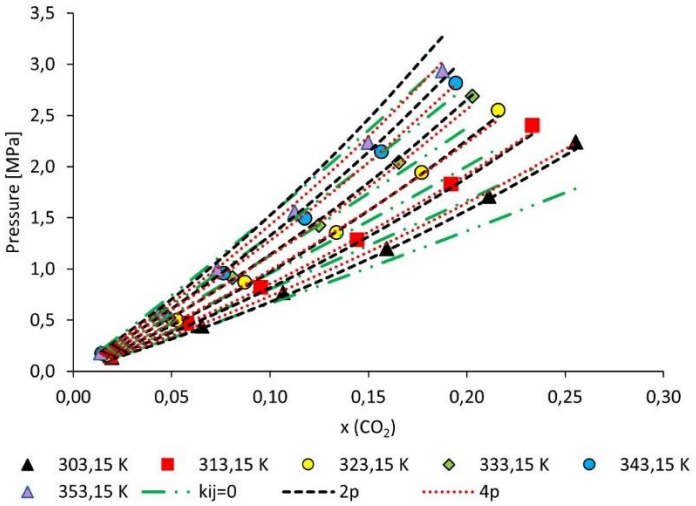

Figure 2. P-x results for CO_2 and [EMIM][TfO] using SRK model with k_{ij}=0, 2p and 4p. Experimental data from Nematpour et al. [14].

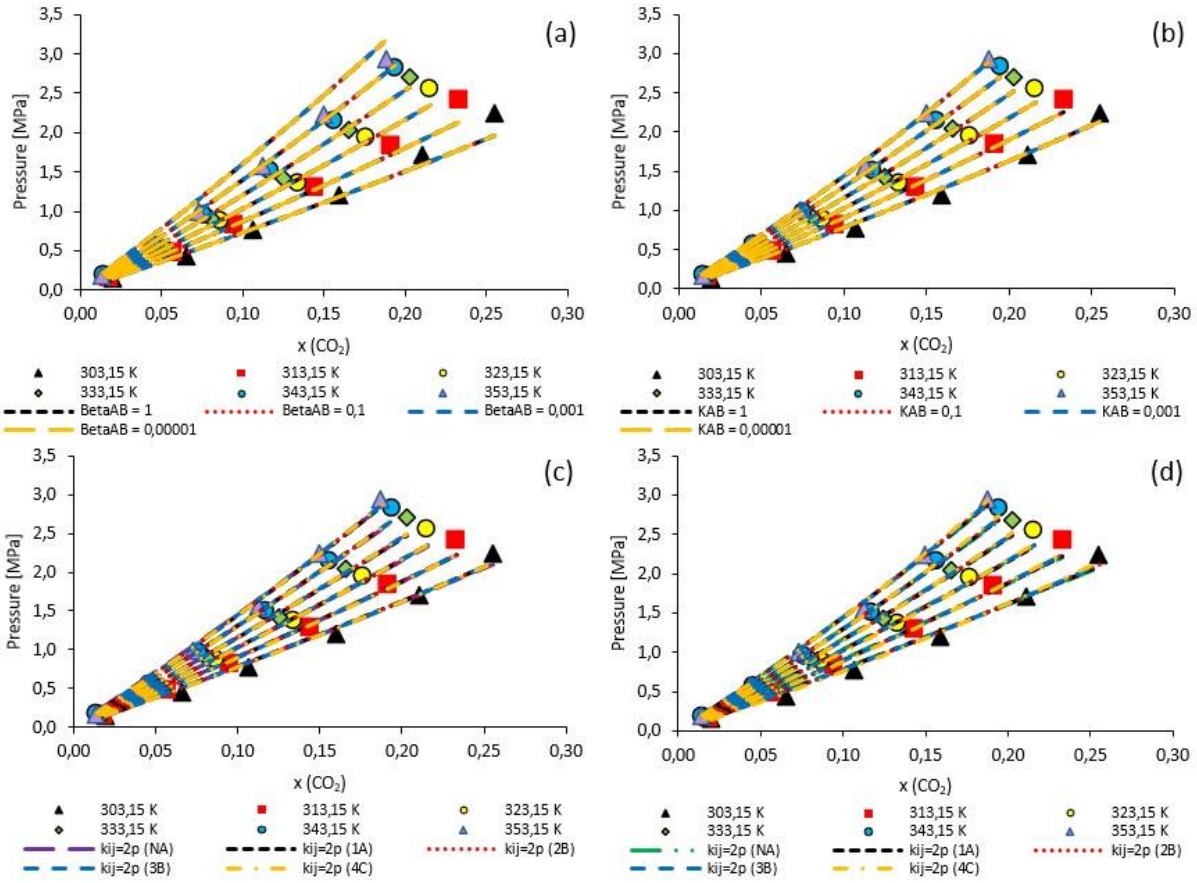

Figure 3. P-x results for CO_2 and [EMIM][TfO]: (a) CPA with different associative parameters (β^{AB}) for the 2B scheme with k_{ij}=0; (b) PC-SAFT with different associative parameters (K^{AB}) for the 2B scheme with k_{ij}=0; (c) Results for CPA EoS with k_{ij}=2p for different associative schemes; (d) Results for PC-SAFT EoS with k_{ij}=2p for different associative schemes. Experimental data from Nematpour et al. [14].

Figure 3(d), respectively, and in the Supplementary Material are presented the AARDs.

For two parameters, the SRK model had AARD of 4.69%, non-associative CPA was 5.81%, CPA (1A) was 5.62%, CPA (2B) and (3B) were 5.43%, and CPA(4C) of 5.07%, while for the non-associative PC-SAFT, it was 5.95%, PC-SAFT (1A) was 5.22%, PC-SAFT (2B) and (3B) was 4.54%, and PC-SAFT (4C) was 3.37% for the same situation. Thus, analyzing the same set of

parameters, the PC-SAFT (4C) EoS had the lowest AARD of 3.37%. On the other hand, when considering the SRK model with four parameters lower deviation is obtained, resulting in an AARD of 2.17%.

For the [OMIM][NTf_2] ionic liquid, we started by performing the solubility curves for the SRK and the CPA (NA) models with k_{ij}=0, which shows a limitation of the EoS in accurately predicting the solubility curves.

After that, adjustments were made to the binary interaction parameters based on phase equilibrium data, in which a significant decrease in AARD was obtained. Thus, adjustments were made to the SRK model with 2 and 4 parameters. And as exposed for the previous ionic liquid, the adjustments made with four parameters significantly reduced the AARD, causing a decrease from 9.71% to 1.12%. It happens because it also uses a binary interaction parameter for the covolume parameter (b), making it a quadratic mixing rule different from the linear mixing rule presented in the CPA EoS.

Furthermore, analyzes were performed using the associative CPA and PC-SAFT models, in which, for this ionic liquid, scheme 1A was the one that presented the best predictive result, being then estimated for the parameter k_{ij} as a function of temperature (k_{ij}=2p). Therefore, in Figure 4, the curves for these models are presented.

In conclusion, the predictive PC-SAFT model showed an excellent fit for the solubility of CO_2 in [OMIM][NTf_2]. With the regression of the binary parameters for the same amount (2 parameters) from the solubility data, the PC-SAFT (4C) model showed the lowest AARD. However, when considering the SRK model with four parameters, it presented the lowest AARD of 1.12%, as shown in the Supplementary Material.

Kontogeorgis and Folas [42] consider induced association (solvation) relevant in mixtures of CO_2+H_2O or CO_2 with methanol or ethanol. However, this application is not considered when considering higher molecular weight alcohols. Mixtures of CO_2 or H_2S and glycols could be well correlated without the need to explicitly explain solvation, for example, for the CO_2-MEG and CO_2-DEG systems, as well as for the CO_2-H_2O-MEG multicomponent mixture. For this reason, since the ILs are not present in the vapor phase, and good results were obtained with the mixtures, there was no interest in adding another parameter.

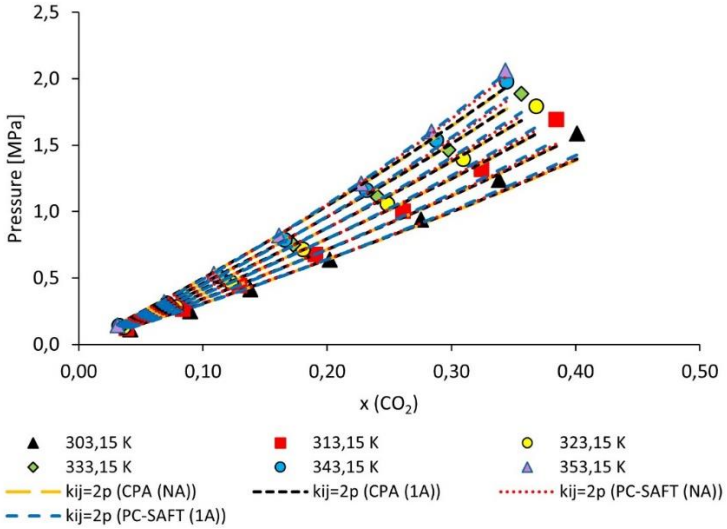

Figure 4. P-x results for CO_2 and [OMIM][NTf_2] for CPA and PC-SAFT EoS with k_{ij}=2p. Experimental data from Jalili et al. [13].

Hydrogen sulfide + ILs equilibria results

Like the presented solubility curves of [EMIM][TfO] and CO_2, the addition of the associative parameter influenced the prediction of the solubility of hydrogen sulfide in the IL, which can be seen in Figure 5(a). Moreover, the same similarity to the previous case can be observed, in which there is no variation in the solubility prediction with the CPA and PC-SAFT EoS with variations in the association parameter.

Differently from what was shown for CO_2 solubility, [EMIM][TfO] using CPA (NA) presented significant errors compared to SRK, and this can be explained by the fact that SRK is not using association for any of the components. At the same time, the CPA was applied with non-association for IL and 3B scheme for H_2S, which leads to the conclusion that in addition to a good parameterization of the IL, the relationship with the association of the other component must be jointly analyzed. Besides, it was important to verify that the addition of associative terms to IL contributed to a better prediction of the solubility curve, presenting

better-calculated values for low H_2S concentrations and higher deviations for higher compositions.

It is possible to observe in Figure 5(b), differently from what is presented for the CPA, that the non-associative PC-SAFT presents a good prediction of the solubility of hydrogen sulfide in the ionic liquid.

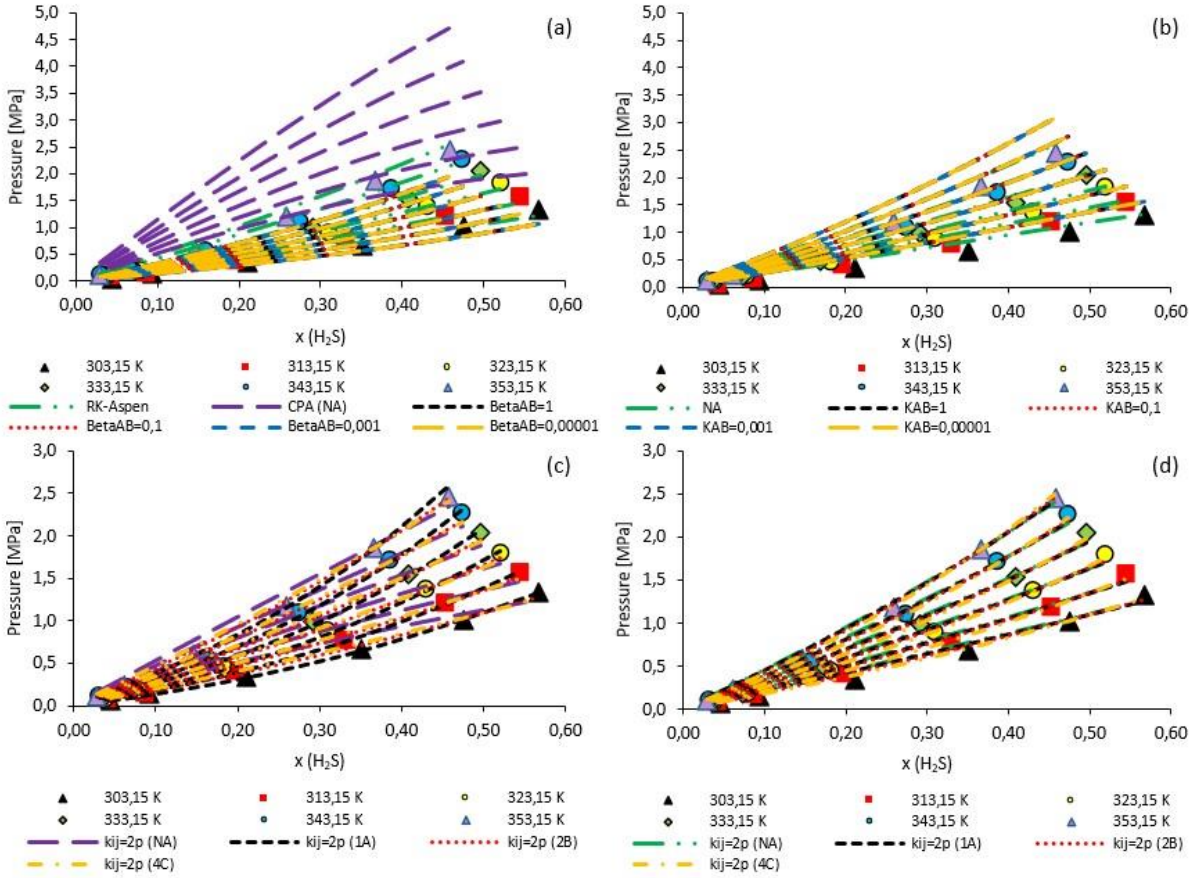

Figure 5. P-x results for H_2S and [EMIM][TfO]: (a) Non-associative and associative CPA with different associative parameters (β^{AB}) for the 2B scheme with k_{ij}=0; (b) Non-associative and associative PC-SAFT EoS with different associative parameters (K^{AB}) for the 2B scheme with k_{ij}=0; (c) Non-associative and associative CPA with different associative schemes with k_{ij}=2p; (d) Non-associative and associative PC-SAFT with different associative schemes with k_{ij}=2p. Experimental data from Nematpour et al. [14].

As previously presented for the mixtures of IL (3B) with CO_2 and CH_4, which were non-associative, it was noticed there were no differences between 2B and 3B schemes. Nonetheless, when analyzing the equilibrium of IL (3B) with H_2S (3B scheme for CPA and 2B scheme for PC-SAFT), it was noticed that the scheme was limited for the prediction of solubility, leading to erroneous equilibrium results. In this context, the 3B associative scheme for ILs has become inappropriate for applications with H_2S. The Aspen plus could not perform the data regression for the CPA EoS, but it was able to perform it for the PC-SAFT. Nevertheless, the results presented were incoherent, thus discarding the possibility of adjusting the parameter k_{ij} for the [EMIM][TfO] (3B). Further details about that scheme are present in the Supplementary Material.

For the CPA and PC-SAFT EoS, data regressions were performed for k_{ij} as a function of temperature for the non-associative and 1A, 2B, and 4C schemes since the 3B scheme has already been evaluated. Therefore, there were significant improvements in the solubility curves from the reduction of the AARD present in the Supplementary Material and verified in Figures 5(c) and 5(d), respectively.

The AARD decreased with the adjustment of the binary interaction parameter, including for the CPA (NA), which presented an AARD of 32.28% (for k_{ij}=0, the deviation was 160.3%). This result showed the impact of modeling H_2S as an associative compound, as in the SRK model, there was no association for H_2S, leading to a reduction in AARD from 160.3% to 18.55%, which was lowered to 1.74%, comparing the predictive with the parameter k_{ij}=4p modes. The other associative CPA schemes showed improvements, in which scheme 1A showed a significant improvement from 20.05% of the predictive to 3.54% for the k_{ij}=2p. The 2B scheme

had 14.39% for the predictive model and 10.48% for the 2p model, and the 4C scheme had 31.99% for the predictive and 15.04% for the k_{ij}=2p model.

In the PC-SAFT EoS, the non-association for IL presented an AARD of 26.49% for the predictive and 18.17% for the model, with k_{ij} adjusted as a function of temperature, i.e., k_{ij}=2p. PC-SAFT (1A) had 29.20% for the predictive and 15.08% for the model with k_{ij}=2p, PC-SAFT 2B had 42.68% for the predictive and 11.87% for the model with k_{ij}=2p, and, finally, the associative 4C scheme showed improvement from 64.83% for the predictive model to 6.56% for the model with k_{ij}=2p.

Figure 6 shows the solubility curves for H_2S in [EMIM][TfO] using the SRK model to verify the effect of the adjustment of the binary interaction parameters for the attractive and covolume parameters.

Figure 6 shows better adjustments with the addition of binary interaction parameters, and for the predictive model, the AARD was 18.55%, while for the parameter k_{ij} with 2p and 4p, it was 2.16% and 1.74%, respectively, showing that the adjustment of the parameter k_{ij} both as a function of temperature and constant values resulted in satisfactory adjustments.

Thus, when evaluating the values of k_{ij} adjusted for 2p, the CPA model (1A) presented the lowest AARD of 3.54%. On the other hand, when considering the

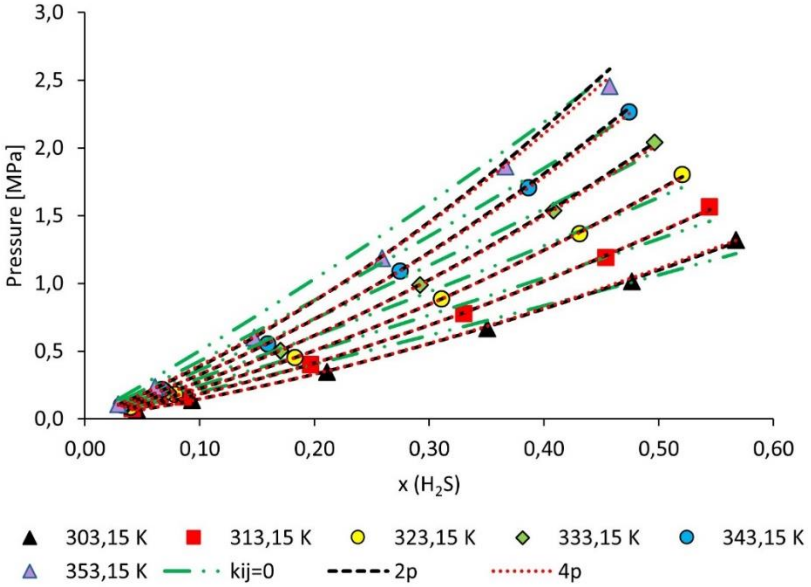

Figure 6. P-x results for H_2S and [EMIM][TfO] using SRK model with k_{ij}=0, 2p and 4p. Experimental data from Nematpour et al. [14].

SRK model adjusted as a function of temperature for the attractive parameter and the covolume parameter for the H_2S solubility curves in [EMIM][TfO], it presented a better fit with AARD of 1.74%.

Among the models analyzed for the [OMIM][NTf_2], the CPA model (2B) showed the lowest AARD for the predictive models, resulting in an AARD of 5.67%. In contrast, the predictive models SRK, CPA (NA), PC-SAFT (NA), and PC-SAFT (2B) showed AARD of 57.51%, 183.69%, 6.78%, and 9.54%, respectively. Furthermore, regressions of the binary interaction parameters of the models mentioned above were performed to improve the solubility curves, thus contributing to a decrease in the AARD.

Analogously to the present for the previous IL, the comparison between the results for the SRK and CPA (NA) models shows that considering H_2S as associative led to much worse predictive results for CPA (NA), however considering H_2S as associative and IL as associative 2B scheme led to better predictive results for CPA than SRK. These results underscore the importance of optimal parameterization for each substance to be designed to work properly together with the other substances in the mixture.

The adjusted SRK model presented AARD for 2p and 4p of 9.53% and 3.51%, respectively, showing that with the adjustment of the binary parameters as a function of temperature, the SRK model was able to represent well the equilibrium data, reducing the predictive AARD from 57.51% to 3.51%, as shown in Figure 7(a).

The CPA (NA) presented an AARD of 11.77%, and the PC-SAFT (NA) indicated a deviation of 5.60%, with two adjusted parameters. Furthermore, for the associative models, CPA and PC-SAFT were analyzed with the same associative schemes, showing that the CPA (2B) had the lowest AARD of 1.81%. The AARD of the PC-SAFT (2B) was 3.48% for two adjusted parameters. These results can be seen in the Supplementary Material.

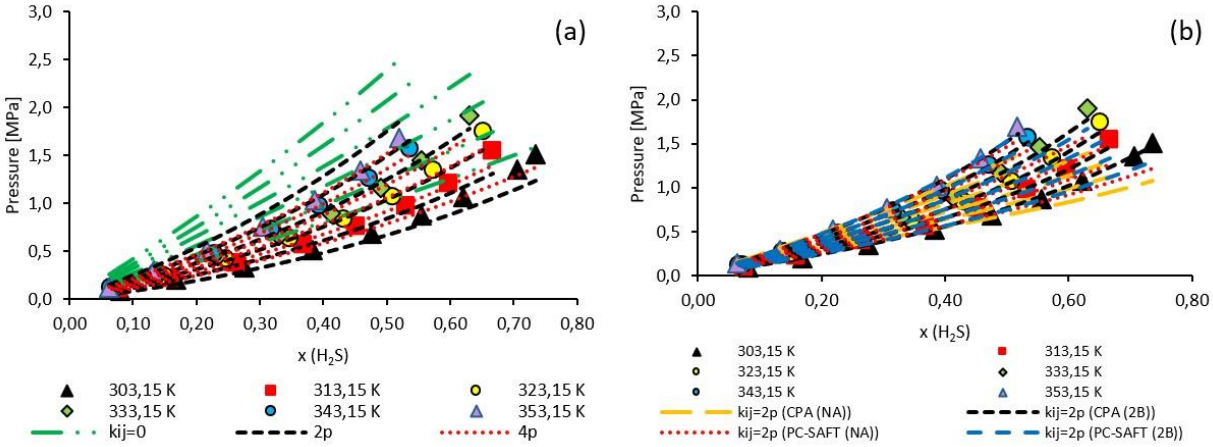

Figure 7. P-x results for H_2S and [OMIM][NTf_2]: (a) Results for SRK model with kij=0, 2p and 4p; (b) Results for SRK, CPA, and PC-SAFT models with k_{ij}=2p. Experimental data from Jalili et al. [13].

In this way, and as shown in Figure 7(b), the models with adjustments of the binary interaction parameter became efficient in correlating the solubility curves. Nonetheless, the CPA model (2B) presented the lowest AARD.

In conclusion to the cases studied, Table 5 summarizes the best models for the cases previously studied using predictive models (k_{ij}=0), and with binary interaction parameters with one and two regressed parameters.

When considering the 4p SRK model, this model showed smaller deviations in all cases, except for the solubility of H_2S in [OMIM][NTf_2], for which the CPA (2B) EoS was the best. Nevertheless, it is worth noting that the SRK model contains more binary parameters than the other models since the covolume parameter of the mixture was adjusted simultaneously.

Table 5. Summary of the best models for ILs with methane and acid gases, in a predictive way (k_{ij}=0) and with the correlation of binary interaction parameters

[EMIM][TfO]			
Components	k_{ij}=0	1p	2p
CH_4	SRK	CPA (NA)	CPA (NA)
CO_2	PC-SAFT (2B)	PC-SAFT (4C)	PC-SAFT (4C)
H_2S	CPA (2B)	CPA (1A)	SRK
[OMIM][NTf_2]			
Components	k_{ij}=0	1p	2p
CO_2	PC-SAFT (1A)	PC-SAFT (1A)	PC-SAFT (4C)
H_2S	CPA (2B)	CPA (2B)	CPA (2B)

CONCLUSION

The SRK model expressed the same behavior as the CPA EoS for the correlation of properties of pure ILs ([EMIM][TfO] and [OMIM][NTf_2]). Nonetheless, for PC-SAFT, the associative effect corroborated the absolute Average Relative Deviation (AARD) decrease in the analyzed properties.

For the [EMIM][TfO] and [OMIM][NTf_2], the PC-SAFT (4C) showed the lowest AARD for density and speed of sound, thus presenting the best fit for both ILs.

For [EMIM][TfO] and the other mentioned components, when adjusting the parameter k_{ij} with 2 parameters, the models that presented the lowest AARD for the system [EMIM][TfO]/CH_4, [EMIM][TfO]/CO_2, and [EMIM][TfO]/H_2S were CPA (NA), PC-SAFT (4C), and SRK, respectively. Furthermore, [OMIM][NTf_2] was analyzed with CO_2 and H_2S with two parameters, and the best models were PC-SAFT (4C) and CPA (2B), respectively.

This present study enabled the thermodynamic modeling of ILs from density and speed of sound data for the SRK, CPA, and PC-SAFT EoS. In addition, this study conceded the addition of ILs in the Aspen plus process simulator. As a result, the data of pure components and mixtures can be explored, allowing their applicability in the simulation of removing acid gases from natural gas.

ACKNOWLEDGEMENT

This work was supported by Coordenação de Aperfeiçoamento de Pessoal de Nível Superior - Brazil (CAPES) under PROC. 88887.633974/2021-00; Fundação de Amparo à Pesquisa do Estado da Bahia

(FAPESB/SECTI/Bahia/Brazil) under Project APP0075/2016 and Conselho Nacional de Desenvolvimento Científico e Tecnológico (CNPq/Brazil) through Grant 303089/2019-9. In addition, the authors acknowledge the financial support provided by Programa de Recursos Humanos da Agência Nacional do Petróleo, Gás Natural e Biocombustíveis – PRH-ANP.

NOMENCLATURE

[BMIM][PF_6]	1-butyl-3-methylimidazolium hexafluorophosphate
[EMIM][FAP]	1-ethyl-3-methylimidazolium Tris(pentafluoroethyl) trifluorophosphate
[EMIM][TfO]	1-ethyl-3-methylimidazolium trifluoromethanesulfonate
[OMIM][NTf_2]	1-octyl-3-methylimidazolium bis(trifluoromethylsulfonyl) imide
AARD	Absolute Average Relative Deviation
CH_4	Methane
CO_2	Carbon dioxide
CPA	Cubic-Plus-Association
DEG	Diethylene glycol
EoS	Equation of state
H_2O	Water
H_2S	Hydrogen sulfide
IL	Ionic liquid
MEG	(Mono)ethylene glycol
NA	Non-associative
N_2	Nitrogen
PC-SAFT	Perturbed-Chain Statistical Associating Fluid Theory
SRK	Soave-Redlich-Kwong
LLE	Liquid-liquid equilibrium
GLE	Gas-liquid equilibria (GLE)

LIST OF SYMBOLS

a_0	Modified alpha function parameter of SRK equation
$a(T)$	Attractive parameter as a function of temperature
$\tilde{a}^{assoc}$	Associative Helmholtz energy
$\tilde{a}^{chain}$	Chain Helmholtz energy
$\tilde{a}^{disp}$	Dispersive Helmholtz energy
$\tilde{a}^{hs}$	Hard-sphere Helmholtz energy
$\tilde{a}^{res}$	Residual Helmholtz energy
a	Attractive mixing parameter
b	Covolume mixing parameter
b_{CPA}	Covolume parameter of CPA
β^{AB}	Association volume of interaction between sites A and B
c_1	Modified alpha function parameter of the SRK equation
C_{1i}	Aspen plus polynomial equations constants
C_{2i}	Aspen plus polynomial equations constants
C_{3i}	Aspen plus polynomial equations constants
C_{4i}	Aspen plus polynomial equations constants
C_{5i}	Aspen plus polynomial equations constants
C_p^{ig}	Ideal gas heat capacity at constant pressure
C_p^{liq}	Liquid heat capacity at constant pressure
C_p^{res}	Residual heat capacity at constant pressure
C_v^{res}	Residual heat capacity at constant volume
δ	Experimental uncertainty
$\Delta^{A_iB_j}$	Strength of interaction between sites A and B
ε_{ij}	Segment energy parameter i and j
ϵ^{AB}	Association energy of interaction between sites A and B
F_{obj}	Objective function
g	Radial distribution function
k_B	Boltzmann's constant
K^{AB}	Parameter of the effective associative volume of PC-SAFT between site A and site B
k_{ij}	Binary interaction
k_{aij}^0	Parameter 0 of binary interaction of component i and j for parameter a of SRK
k_{aij}^1	Parameter 1 of binary interaction of component i and j for parameter a of SRK
k_{bij}^0	Parameter 0 of binary interaction of component i and j for parameter b of SRK
k_{bij}^1	Parameter 1 of binary interaction of component i and j for parameter b of SRK
k_{ij}^0	Parameter 0 of binary interaction of components i and j for CPA and PC-SAFT models
k_{ij}^1	Parameter 1 of binary interaction of components i and j for CPA and PC-SAFT models
m_i	Segment number i
m_m	"Monomer" parameter
MM	Molar mass
n	Total number of elements

σ_i Segment diameter i

Ω_A Parameter of the SRK EoS, $\Omega_A = 0.42748$

Ω_B Parameter of the SRK EoS, $\Omega_B = 0.08664$

P Pressure

P_{Ant}^{v} Antoine's pressure

P_c^* Critical pressure adapted from SRK

P_{cm} "monomer" critical pressure

ρ Density

ρ_i^{cal} Calculated density of component i

ρ_i^{exp} Experimental density of component i

R Gas constant

T Temperature

T_c^* Critical temperature adapted from SRK

T_{cm} "monomer" critical temperature

T_{ref} Reference temperature, $T_{ref} = 298.15$ K

u_i^{cal} Calculated density of component i

u_i^{exp} Experimental density of component i

V_m Mole volume

v_i^{exp} Experimental variable

v_i^{cal} Calculated variable

ω Acentric factor

X_{A_i} Mole fraction of the compound not bonded at site A

x_i Mole fraction of component i

x_j Mole fraction of component j

REFERENCES

[1] I. Iliuta, F. Iarachi, Int. J. Greenhouse Gas Control 79 (2018) 1–13. https://doi.org/10.1016/j.ijggc.2018.09.016.

[2] J. Carrol, Natural Gas Hydrates: A Guide for Engineers, 4. Ed., Gulf Professional Publishing (2020) p. 377. ISBN: 978-0-12-821771-9.

[3] A. Haghtalab, A. Afsharpour, Fluid Phase Equilib. 406 (2015) 10–20. https://doi.org/10.1016/j.fluid.2015.08.001.

[4] J. Haider, S. Saeed, M.A. Qyyum, B. Kazmi, R. Ahmad, A. Muhammad, M. Lee, Renewable Sustainable Energy Rev. 123 (2020) 109771. https://doi.org/10.1016/j.rser.2020.109771.

[5] R. Santiago, J. Lemus, A.X. Outomuro, J. Bedia, J. Palomar, Sep. Purif. Technol. 233 (2020) 116050. https://doi.org/10.1016/j.seppur.2019.116050.

[6] G. Yu, C. Dai, L. Wu, Z. Lei, Energy Fuels 31 (2017) 1429–1439. https://doi.org/10.1016/j.gee.2020.10.022.

[7] S.E. Sanni, O. Agboola, O. Fagbiele, E.O. Yusuf, M.E. Emetere, Egypt. J. Pet. 29 (2020) 83–94. https://doi.org/10.1016/j.ejpe.2019.11.003.

[8] T.E. Akinola, E. Oko, M. Wang, Fuel 236 (2019) 135–146. https://doi.org/10.1016/j.fuel.2018.08.152.

[9] K. Huang, X.-M. Zhang, Y. Xu, Y.-T. Wu, X.-B. Hu, AIChE J. 60 (2014) 4232–4240. https://doi.org/10.1002/aic.14634.

[10] S. Zhang, J. Zhang, Y. Zhang, Y. Deng, Chem. Rev. 117 (2017) 6755–6833. https://doi.org/10.1021/acs.chemrev.6b00509.

[11] S.K. Singh, Int. J. Biol. Macromol. 132 (2019) 265–277. https://doi.org/10.1016/j.ijbiomac.2019.03.182.

[12] M. Freemantle, Chem. Eng. News 78 (2000) 37–50. https://doi.org/10.1021/cen-v078n020.p037.

[13] A.H. Jalili, M. Safavi, C. Ghotbi, A. Mehdizadeh, M. Hosseini-Jenab, V. Taghikhani, J. Phys. Chem. B 116 (2012) 2758–2774. https://doi.org/10.1021/jp2075572.

[14] M. Nematpour, A.H. Jalili, C. Ghotbi, D. Rashtchian, J. Nat. Gas Sci. Eng. 30 (2016) 583–591. https://doi.org/10.1016/j.jngse.2016.02.006.

[15] A.K. Jana, Process simulation and control using AspenTM, PHI Learning Private Limited, (2009) p. 317. ISBN: 978-81-203-3659-9.

[16] A.M. Law, W. D. Kelton, Simulation modeling & analysis, 2. ed., McGraw-Hill International editions, (1991) p. 672. ISBN-13: 978-0070366985.

[17] A.I. Papadopoulos, I. Tsivintzelis, P. Linke, P. Seferlis, in Elsevier Reference Module in Chemistry, Molecular Sciences and Chemical Engineering, Elsevier (2018) https://doi.org/10.1016/B978-0-12-409547-2.14342-2.

[18] L.F. Cardona, J.O. Valderrama, J. Mol. Liq. 317 (2020) 113926. https://doi.org/10.1016/j.molliq.2020.113926.

[19] G. Soave, Chem. Eng. Sci. 27 (1972) 1197–1203. https://doi.org/10.1016/0009-2509(72)80096-4.

[20] M.S. Graboski, T.E. Daubert, Ind. Eng. Chem. Process Des. Dev. 18 (1979) 300–306. https://doi.org/10.1021/i260070a022.

[21] P.M. Mathias, Ind. Eng. Chem. Process Des. Dev. 22 (1983) 385–391. https://doi.org/10.1021/i200022a008.

[22] G.M. Kontogeorgis, E.C. Voutsas, I. V. Yakoumis, D.P. Tassios, Ind. Eng. Chem. Res. 35 (1996) 4310–4318. https://doi.org/10.1021/ie9600203.

[23] G.M. Kontogeorgis, M.L. Michelsen, G.K. Folas, S. Derawi, N. Von Solms, E.H. Stenby, Ind. Eng. Chem. Res. 45 (2006) 4855–4868. https://doi.org/10.1021/ie051305v.

[24] S. Huang, M. Radosz, Ind. Eng. Chem. Res. 29 (1990) 2284–2294. https://doi.org/10.1021/ie00107a014.

[25] J. Gross, G. Sadowski, Ind. Eng. Chem. Res. 40 (2001) 1244–1260. https://doi.org/10.1021/ie0003887.

[26] S.F. Baygi, H. Pahlavanzadeh, Chem. Eng. Res. Des. 93 (2015) 789–799. https://doi.org/10.1016/j.cherd.2014.07.017.

[27] J. Gross, G. Sadowski, Ind. Eng. Chem. Res. 41 (2002) 5510–5515. https://doi.org/10.1021/ie010954d.

[28] W.G. Chapman, K.E. Gubbins, G. Jackson, M. Radosz, Ind. Eng. Chem. Res. 29 (1990) 1709–1721. https://doi.org/10.1021/ie00104a021.

[29] J. Gross, O. Spuhl, F. Tumakaka, G. Sadowski, Ind. Eng. Chem. Res. 42 (2003) 1266–1274. https://doi.org/10.1021/ie020509y.

[30] M. Loreno, R.A. Reis, S. Mattedi, M.L.L. Paredes, Fluid Phase Equilib. 479 (2019) 85–98. https://doi.org/10.1016/j.fluid.2018.09.010.

[31] E. Vercher, A.V. Orchillés, P.J. Miguel, A. Martínez-

Andreu, J. Chem. Eng. Data 52 (2007) 1468–1482. https://doi.org/10.1021/je7001804.
[32] B-C. Lee, Korean J. Chem. Eng. 54 (2016) 213–222. https://doi.org/10.9713/kcer.2016.54.2.213.
[33] E. Zorębski, M. Geppert-Rybczńska, M. Zorębski, J. Phys. Chem. B 117 (2013) 3867–3876. https://doi.org/10.1021/jp400662w.
[34] J. Kennedy, R. Eberhart, Proc. ICNN'95 Int. Conf. N. Net. (1995) 1942–1948. https://doi.org/10.1109/ICNN.1995.488968.
[35] J.A. Nelder, R. Mead, Comp. J. 7 (1965) 308–313. https://doi.org/10.1093/comjnl/7.4.308.
[36] R.J. Topliss, D. Dimitrelis, J. M. Prausnitz, Comput. Chem. Eng. 12 (1988) 483–489. https://doi.org/10.1016/0098-1354(88)85067-1.
[37] Aspen plus 2019 - Aspen Technology Inc. – USA.
[38] I. Tsivintzelis, G.M. Kontogeorgis, M.L. Michelsen, E.H. Stenby, AIChE J. 56 (2010) 2965–2982. https://doi.org/10.1002/aic.12207.
[39] L. Ruffine, P. Mougin, A. Barreau, Ind. Eng. Chem. Res. 45 (2006) 7688–7699. https://doi.org/10.1021/ie0603417.
[40] X. Tang, J. Gross, Fluid Phase Equilib. 293 (2010) 11–21. https://doi.org/10.1016/j.fluid.2010.02.004.
[41] Nist, NIST Livro de Química na Web, https://webbook.nist.gov/chemistry/ [Accessed 09 august 2021].
[42] G.M. Kontogeorgis, G.K. Folas, Thermodynamic Models for Industrial Applications, 1. Ed., John Wiley & Sons Inc(2010) p. 710. ISBN: 978-0-470-69726-9

LUCAS OLIVEIRA CARDOSO[1]
BRUNO SANTOS CONCEIÇÃO[1]
MÁRCIO LUIS LYRA PAREDES[2]
SILVANA MATTEDI[1]

[1]Chemical Engineering Graduate Program (UFBA/UNIFACS), Polytechnic School, Federal University of Bahia, Salvador, BA, Brazil

[2]Chemical Engineering Graduate Program, Rio de Janeiro State University, Rio de Janeiro, RJ, Brazil

NAUČNI RAD

TERMODINAMIČKO MODELOVANJE RASTVORLJIVOSTI GASOVA U JONSKIM TEČNOSTIMA KORISTEĆI JEDNAČINE STANJA

Ovaj rad je usmeren na termodinamičko modelovanje rastvorljivosti gasova u jonskim tečnostima koristeći sledeće jednačine stanja: Soave-Redlich-Kwong (SRK), Cubic-Plus-Association (CPA) i Perturbed-Chain Statistical Associating Fluid Theory (PC-SAFT). Zbog toga su razvijene rutinske metode parametrizacije jonskih tečnosti. Zatim su jonske tečnosti implementirane u simulatoru Aspen plus da bi procenili jednačine stanja i istražili podatke za ravnotežu faza prediktivnim jednačinama i korelacijom parametra binarne interakcije. Tako je verifikovana korelacija gustine, dok su krive brzine zvuka imale ograničenja za ispravljanje nagiba krivih za čiste jonske tečnosti. Bez obzira na to, jednačina stanja PC-SAFT sa asocijativnom šemom 4C pokazala ee prikladnijom za termofizička svojstva. Što se tiče predviđanja ravnoteže faze za [EMIM] [TFO], jednačina stanja PC-SAFT sa 2B šemom pokazala se boljom za CO_2, dok je jednačina stanja CPA sa 2B šemom imala najbolji rezultat za H_2S. Za [OMIM] [NTF_2], jednačina stanja PC-SAFT sa 1A šemom pokazala je bolje rezultate za CO_2, a jednačina stanja CPA sa 2B šemom pokazala je najmanje odstupanje za H_2S.

Ključne reči: termodinamičko modelovanje, jonske tečnosti, jednačine stanja, povezivanje, Aspen plus.